



**HAL**  
open science

# Spectroscopic characterisation of hydroxyapatite and nanocrystalline apatite with grafted aminopropyltriethoxysilane: nature of silane–surface interaction

Audric Michelot, Stéphanie Sarda, Catherine Audin, Éric Deydier, Eric Manoury, Rinaldo Poli, Christian Rey

## ► To cite this version:

Audric Michelot, Stéphanie Sarda, Catherine Audin, Éric Deydier, Eric Manoury, et al.. Spectroscopic characterisation of hydroxyapatite and nanocrystalline apatite with grafted aminopropyltriethoxysilane: nature of silane–surface interaction. *Journal of Materials Science*, 2015, 50 (17), pp.5746-5757. 10.1007/s10853-015-9122-x . hal-01490593

**HAL Id: hal-01490593**

**<https://hal.science/hal-01490593>**

Submitted on 15 Mar 2017

**HAL** is a multi-disciplinary open access archive for the deposit and dissemination of scientific research documents, whether they are published or not. The documents may come from teaching and research institutions in France or abroad, or from public or private research centers.

L'archive ouverte pluridisciplinaire **HAL**, est destinée au dépôt et à la diffusion de documents scientifiques de niveau recherche, publiés ou non, émanant des établissements d'enseignement et de recherche français ou étrangers, des laboratoires publics ou privés.



## Open Archive Toulouse Archive Ouverte (OATAO)

OATAO is an open access repository that collects the work of Toulouse researchers and makes it freely available over the web where possible.

This is an author-deposited version published in: <http://oatao.univ-toulouse.fr/>  
Eprints ID: 16540

To link to this article: DOI:10.1007/s10853-015-9122-x

<http://dx.doi.org/10.1007/s10853-015-9122-x>

**To cite this version:**

Michelot, Audric and Sarda, Stéphanie and Audin, Catherine and Deydier, Eric and Manoury, Eric and Poli, Rinaldo and Rey, Christian  
*Spectroscopic characterisation of hydroxyapatite and nanocrystalline apatite with grafted aminopropyltriethoxysilane: nature of silane–surface interaction.* (2015) *Journal of Materials Science*, vol. 50 (n°17). pp. 5746-5757. ISSN 0022-2461

Any correspondence concerning this service should be sent to the repository administrator: [staff-oatao@listes-diff.inp-toulouse.fr](mailto:staff-oatao@listes-diff.inp-toulouse.fr)

# Spectroscopic characterisation of hydroxyapatite and nanocrystalline apatite with grafted aminopropyltriethoxysilane: nature of silane–surface interaction

Audric Michelot<sup>1,2</sup> · Stéphanie Sarda<sup>1</sup> · Catherine Audin<sup>2,3</sup> · Eric Deydier<sup>2,3</sup> · Eric Manoury<sup>2,3</sup> · Rinaldo Poli<sup>2,3,4</sup> · Christian Rey<sup>5</sup>

**Abstract** Heterogenised homogeneous catalysis is commonly performed with molecular catalysts grafted on solids via adsorption or via a covalent molecular link. Covalent grafting of organic groups on solid supports is usually carried out by silylation, using functionalised trialkoxysilanes. Among these solids supports, very few studies have been published on apatites. In the present work, aminopropyltriethoxysilane (APTES) grafting was performed in toluene on different apatitic supports: crystallised stoichiometric hydroxyapatites differing by the drying method, freeze-dried (HAP) and dried at 100 °C (HAPD), and a nanocrystalline apatite. All materials were fully characterised, before and after grafting, for better understanding of the nature of the alkoxy silane/surface interaction. The data show a clear competition between the covalent grafting of APTES and its polycondensation reaction, depending on the nature of the solid support surface. Silylation is accompanied by APTES covalent grafting to oxygen atom of the hydroxyl groups of the apatitic structure and/or of the OH<sup>-</sup> species that are present on the surface hydrated layer. This work clarifies the nature of silane grafting onto selected apatitic surfaces and

especially the influence of the composition and properties of the apatitic surfaces on the process of silylation.

## Introduction

The development of supported molecular catalyst is nowadays a major field in catalysis research. Heterogeneous catalysis appears as an alternative method in organic synthesis as it presents several advantages over homogeneous processes, including simple product isolation as well as catalyst separation and recycling [1]. Heterogenised homogeneous catalysis is commonly performed with molecular catalysts grafted on solids via adsorption or via a covalent molecular link. The interest of supported catalysis is to combine the activity and selectivity of homogeneous catalysts with the easy recovery of solids, which is of particular interest in asymmetric catalysis. The solid supports may be organic (polymers) or inorganic.

The most commonly used inorganic solid for supported heterogeneous catalysis is silica, but other inorganic solids such as metallic oxides or ceramics [1], and more recently apatite calcium phosphates (or apatites), have also been reported as suitable and very promising supports. Among these different solids, very few studies have been published on apatites. Apatites constitute the mineral part of calcified tissues, such as bone and teeth, and are widely used in biomedical applications such as implant coatings, bioceramics, or bone cements thanks to their excellent biocompatibility, bioactivity, and osteoconductive properties [2–4]. Moreover, they present high ion-exchange ability and adsorption capacity. Thus, modified apatites have been investigated not only for biomaterial applications but also as delivery systems for molecules of biological interest such as proteins [5], growth factors [6], and drugs [7], as

& Stéphanie Sarda  
stephanie.sarda@iut-tlse3.fr

<sup>1</sup> CIRIMAT, INPT-CNRS-UPS, Université de Toulouse, Université Paul Sabatier, 4 Allée Emile Monso, BP 44362, 31030 Toulouse Cedex 04, France

<sup>2</sup> CNRS, LCC, 31077 Toulouse Cedex 04, France

<sup>3</sup> Université de Toulouse, Université Paul Sabatier, INPT, 31077 Toulouse Cedex 04, France

<sup>4</sup> Institut Universitaire de France, 75005 Paris, France

<sup>5</sup> CIRIMAT, INPT-CNRS-UPS, Université de Toulouse, ENSIACET, 31030 Toulouse Cedex 04, France

adsorbents for heavy metals in environmental applications [8], in chromatography column separations systems [9], and as supports for heterogeneous catalysis [10, 11].

Covalent grafting of organic groups on solid support is usually carried out by silylation, using functionalised trialkoxysilanes  $(\text{OR}^0)_3\text{SiR}$ . R is an alkyl- or aryl-functionalised chain and  $\text{Si}(\text{OR}^0)$  is a hydrolysable function,  $\text{R}^0$  being most frequently a methyl or an ethyl group. On the one hand, the  $\text{Si}(\text{OR}^0)$  bond is easily hydrolyzed in aqueous solution with the elimination of alcohol ( $\text{R}^0\text{-OH}$ ) to form metastable silanol ( $-\text{SiOH}$ ), which undergoes condensation to more stable siloxane ( $\text{Si-O-Si}$ ), forming three-dimensional hyperbranched oligomers [12]. On the other hand, with solids bearing surface OH groups (solid-OH), a monolayer or covalently grafting solid- $\text{OSi}(\text{OH})_2\text{R}$  can be achieved in anhydrous media [13]. This is a well-known and efficient strategy for silica-controlled grafting. The use of non-polar organic solvents during the surface modification of silica surfaces with 3-aminopropyltriethoxysilane (APTES) leads to the formation of stable surface layers by covalent interactions [14, 15].

Among compounds of the apatitic calcium phosphate family, hydroxyapatite (HAP),  $\text{Ca}_{10}(\text{PO}_4)_6(\text{OH})_2$ , is a widely studied compound. It is the stoichiometric apatitic calcium phosphate (Ca/P atomic ratio of 1.67) which is characterised by low solubility in water, low cost, and high innocuousness. Moreover, thanks to the presence of structural hydroxyl groups, HAP is a good candidate for surface functionalisation using alkoxy silane agents [8, 16]. APTES is a widely used reagent for surface functionalisation of inorganic solid [1], bearing both a trialkoxysilane group (surface anchor) and an amine function allowing an easy coupling with various organic molecules via nucleophilic substitution. This reagent has been used with success for silica and HAP grafting for immobilisation of a large variety of molecules or proteins [13]. Recently published papers reported that APTES reacts with HAP via condensation of the hydrolyzed ethoxy moieties with the hydroxyl groups found at the surface of the HAP [13, 16]. Some studies have also highlighted the influence of the reaction conditions, such as time, temperature [16], or the morphology [17] of apatitic crystals on the interaction between APTES and the HAP surface. However, none of these published works reported the effect of the chemical nature and crystallinity of the apatitic supports. Moreover, the use of nonstoichiometric nanocrystalline apatites (NCA,  $\text{Ca}_{10-x}(\text{PO}_4)_{6-x}(\text{HPO}_4 \text{ or } \text{CO}_3)_x(\text{OH})_{2-x}$  with  $0 < x < 1$  and a Ca/P molar ratio ranging from 1.50 to 1.67), which present a greater surface area than HAP and a structured hydrated layer on their surface, rich in surface labile species able to be exchanged [18], has been poorly studied [19, 20].

The aim of this work is to address these two points: to explore the influence of APTES grafting on the chemical

composition and the crystallinity of two calcium phosphate materials (crystallised stoichiometric hydroxyapatite, HAP, and a nanocrystalline apatite, NCA) and to characterise the trialkoxysilane–solid surface interaction that is still poorly understood. APTES grafting was performed in toluene on both materials. All materials were fully characterised, before and after grafting, by different techniques and especially by FTIR, Raman, and NMR spectroscopy.

## Experimental section

### Materials

The well-crystallised stoichiometric hydroxyapatite powders were synthesised by a double decomposition technique between  $(\text{NH}_4)_2\text{HPO}_4$  (433.3 mL, 1.54 M in deionised water) and  $\text{Ca}(\text{NO}_3)_2 \cdot 4\text{H}_2\text{O}$  (1100 mL, 1 M in deionised water) at 90 °C and pH around 10 for about 3 h [21]. After filtration and washing, the precipitate was either freeze-dried (HAP) or dried at 100 °C for 5 h in a vacuum to remove the residual physisorbed water (HAPD). Then the powder was sieved ( $\phi 125 \mu\text{m}$ ) and stored in a freezer.

Nanocrystalline apatite powder (NCA) was prepared by a double decomposition technique at ambient temperature (pH close to 7) between  $(\text{NH}_4)_2\text{HPO}_4$  (1500 mL, 0.60 M in deionised water) and  $\text{Ca}(\text{NO}_3)_2 \cdot 4\text{H}_2\text{O}$  (750 mL, 0.29 M in deionised water) [22]. The precipitate obtained in few minutes was filtered, washed, and freeze-dried. Then the powder was sieved ( $\phi 125 \mu\text{m}$ ) and stored in a freezer.

(3-Aminopropyl)triethoxysilane (APTES, 98 %, Sigma-Aldrich) was used without further purification.

### Grafting experiments

The grafting of APTES on HAP, HAPD, and NCA was carried out according to published methods [17, 23]. Under an inert argon atmosphere, anhydrous toluene (20 mL) was added to the apatitic particles (1 g) together with APTES (2.33 mL). The mixture was refluxed at 110 °C overnight. The solid products were separated by centrifugation, washed three times with toluene and twice with ether, and dried at 70 °C under vacuum overnight. The obtained APTES-grafted apatites were designated as HAP-Si, HAPD-Si, and NCA-Si.

For each apatitic support, blank experiments were performed under the same experimental conditions without APTES; these blanks were designated as HAP0, HAPD0, and NCA0.

The same experiments were performed by adding water to the toluene suspension containing HAP and APTES to favor polymerisation of the surface agent. The sample obtained was designated as HAP-Si-Poly.

## Characterisation techniques

Elemental analyses were performed with a Perkin-Elmer 2400 instrument. The phosphate content of the synthesised apatites was determined by UV–visible spectroscopy of the phosphovanadomolybdic acid complex and the calcium content by complexometry with ethylenediaminetetraacetic acid [24]. The estimated standard deviations of calcium and phosphate titrations were equivalent to 1 % of the reading. The specific surface area was measured by the Brunauer–Emmett–Teller (BET) method with a Quantachrome Instruments Monosorb Nova 1000 with an estimated standard deviation of 0.5 m<sup>2</sup>/g.

The amount of water in the powders was measured by thermogravimetric analysis (TGA-DTA) using TA instruments Q600 from 25 °C up to 1000 °C at a heating rate of 5 °C/min under an air flux (30.00 ± 0.01 mg of each sample).

The solid phases before and after grafting APTES were characterised by X-ray diffraction (XRD) (BRUKER D8-2 diffractometer CuK $\alpha$ 1 radiation with  $k = 1.5406 \text{ \AA}$ ). The apparent crystallite sizes were calculated from the (310) and (002) lines by applying Scherrer's formula [25].

Transmission electron microscopy (TEM) micrographs of the powders before and after grafting were recorded in the bright-field imaging on a JEOL JEM 2100F microscope set at an acceleration tension of 200 kV.

Unmodified and modified particles were characterised by several spectroscopic techniques. Fourier transform infrared (FTIR) analyses were performed with an Impact 400 Nicolet FTIR spectrometer. All adsorption spectra were obtained by accumulation of 32 scans at a 4 cm<sup>-1</sup> resolution covering the 4000–400 cm<sup>-1</sup> range (2 mg sample/300 mg KBr).

Raman spectroscopy analyses were carried out with a Horiba, Jobin–Yvon Labram HR800 confocal microspectrometer ( $k = 532 \text{ nm}$ ). The spectral resolution was 2 cm<sup>-1</sup>, the laser was power 2 mW, integration times varied from 30 to 60 s, and spectral accumulations from 2 to 30, over a wavenumber range of 100–4000 cm<sup>-1</sup>.

<sup>29</sup>Si, <sup>13</sup>C, and <sup>31</sup>P cross-polarisation magic angle spinning (CP-MAS) solid-state NMR spectra were recorded at 79.39, 100.49, and 161.74 MHz, respectively. <sup>1</sup>H MAS NMR spectra were recorded at 399.61 MHz. All experiments were realised with a spinning rate of 8 kHz on a Bruker Avance 400 spectrometer (9.4 T).

## Results

### Characterisation of the apatitic samples

Chemical analyses of the synthesised solids gave a Ca/P ratio of 1.66 ± 0.02 for the HAP and HAPD samples

corresponding to stoichiometry hydroxyapatite (Ca<sub>10</sub>(PO<sub>4</sub>)<sub>6</sub>(OH)<sub>2</sub>), whereas NCA displayed a Ca/P ratio of 1.40 ± 0.02, characteristic of a calcium-deficient apatite.

The water content was determined by thermogravimetric analysis (TGA) in the temperature range of 25–1000 °C. TGA showed a two-stage weight loss of water between 25 and 400 °C, attributed to adsorbed and lattice water on HAP [26, 27]. As expected, due to its hydrated surface layer, NCA presented the highest water content (15.00 ± 0.20 wt%). It decreased from HAP (4.00 ± 0.04 wt%) to HAPD (1.50 ± 0.02 wt%) due to the different drying procedure.

The specific surface areas of the stoichiometric apatites HAP and HAPD are lower than that of NCA: 58 (±3), 52 (±3), and 101 (±5) m<sup>2</sup>/g, respectively. These results are in accordance with TEM observations (Fig. 1). Both samples crystallise as small needles (longer needles for HAP samples than for NCA) with a thickness of fewer than 100 nm.

The HAP and HAPD powders exhibited well-defined XRD patterns (Fig. 2a) corresponding to well-crystallised apatitic calcium phosphates, whereas NCA exhibited broad peaks due to the low crystallinity of the apatitic phase [18]. No additional crystalline phase was detected. The apparent crystallite sizes were calculated from XRD using Scherrer's equation [25] from the (310) and (002) lines, and the results are reported in Table 1. All the crystals were elongated along the *c*-axis of the hexagonal structure in accordance with the TEM observations. The crystallites sizes observed for NCA appear lower than for hydroxyapatites samples, in accordance with TEM observations (Fig. 1).

The FTIR spectra of HAP and HAPD showed the characteristic bands of apatitic calcium phosphate (Fig. 3a): apatitic PO<sub>4</sub><sup>3-</sup> vibration bands at 473 cm<sup>-1</sup> (*m*<sub>2</sub>), 560–630 cm<sup>-1</sup> (*m*<sub>4</sub>), 962 cm<sup>-1</sup> (*m*<sub>1</sub>), and 1000–1100 cm<sup>-1</sup> (*m*<sub>3</sub>) and OH bands at 630 and 3560 cm<sup>-1</sup>, characteristic of an apatitic environment [28]. For HAP and HAPD, a weak and broad band between 1420 and 1470 cm<sup>-1</sup> due to the low number of carbonate ions and a weak band at 875 cm<sup>-1</sup> assigned to both carbonate and possibly HPO<sub>4</sub><sup>2-</sup> ions were observed, suggesting that the powders could be a slightly calcium-deficient hydroxyapatite. As expected, these CO<sub>3</sub><sup>2-</sup> and HPO<sub>4</sub><sup>2-</sup> vibration bands, as well as the free water vibration bands (1630 and 3400 cm<sup>-1</sup>), were much more intense for the NCA particles. Moreover, the FTIR spectrum of NCA exhibited broader apatitic phosphate bands, characteristic of a poorly crystalline apatite [18] with weak carbonate bands. Curve fitting analysis in the *m*<sub>4</sub>PO<sub>4</sub> domain using the GRAMS/386 software (Fig. 3b) confirmed the formation of biomimetic nanocrystalline apatite with non-apatitic environments of PO<sub>4</sub><sup>3-</sup> (620 cm<sup>-1</sup>) and HPO<sub>4</sub><sup>2-</sup> (530 cm<sup>-1</sup>) ions present in the hydrated surface layer [29]. Weak OH vibrations were detected on the curve-fitted spectrum of NCA suggesting a

Fig. 1 TEM observations of HAP and NCA before and after grafting

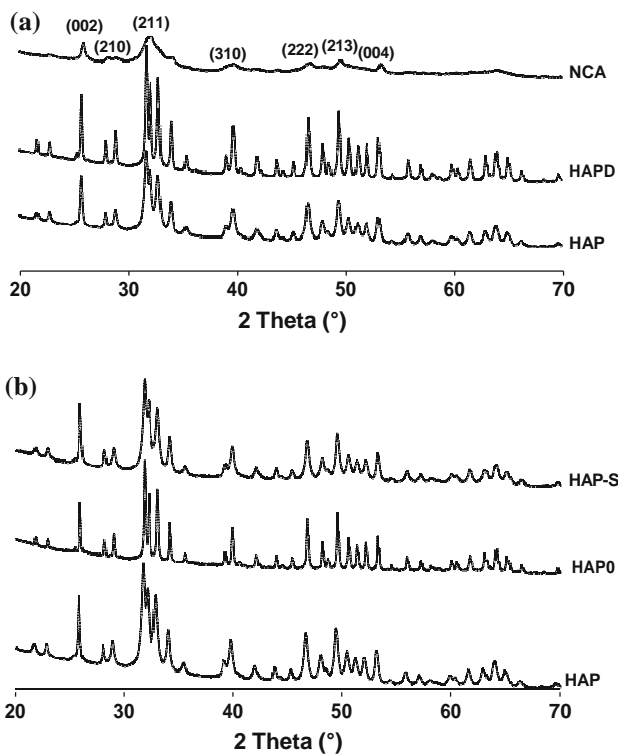
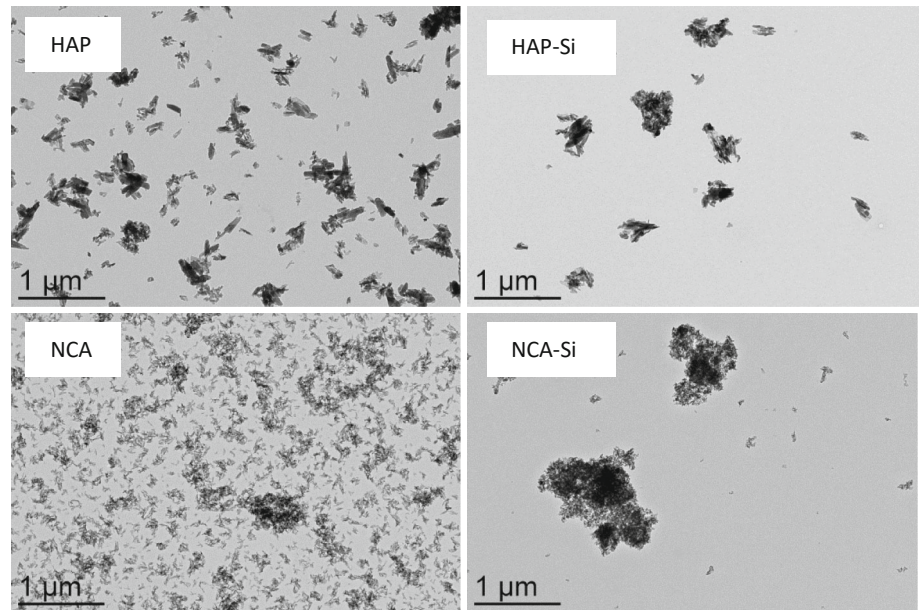


Fig. 2 X-ray diffraction diagrams of a HAP, HAPD, and NCA before grafting; b HAP before and after grafting (HAP-Si) and blank experiments (HAP0)

very low hydroxide ion content related to the calcium deficiency [27].

The Raman spectra of HAP (Fig. 4a), HAPD, and NCA synthesised powders presented characteristic lines of apatitic phosphate groups in accordance with the FTIR studies:

the  $m_1$  ( $960\text{ cm}^{-1}$ ),  $m_2$  ( $430\text{--}450\text{ cm}^{-1}$ ),  $m_3$  ( $1040\text{--}1074\text{ cm}^{-1}$ ), and  $m_4$  ( $580\text{--}608\text{ cm}^{-1}$ ) modes of  $\text{PO}_4^{3-}$  [18]. For NCA (data not shown), phosphate bands were broader and an additional vibration mode of  $\text{HPO}_4^{2-}$  at  $875\text{ cm}^{-1}$  was observed [30].

The CP-MAS  $^{31}\text{P}$  solid NMR spectra of the synthesised HAP are shown in Fig. 5a. As expected, the highly crystalline HAP presented a relatively sharp signal at 3.0 ppm corresponding to orthophosphate species [31]. For the NCA sample (data not shown), a characteristic broader asymmetric signal was observed due to the presence of  $\text{HPO}_4^{2-}$  species. The broadening of the signal could also be attributed to the nanoscopic nature of the sample [32]. The MAS  $^1\text{H}$  solid NMR spectrum of HAP (Fig. 5b) displayed a signal at -0.2 ppm attributed to the OH groups of the apatitic structure and a broader one at 5.1 ppm attributed to adsorbed water molecules [18, 31]. NCA displayed more complex spectra (data not shown) as this structure contains a higher concentration of water and hydrogen phosphates both giving broad signals at around 5 and 14 ppm, respectively. Several lines were also observed between 2 and 5 ppm; these were also mentioned by other groups, but their structural origin remains unclear [32].

### Characterisation after silylation

In order to analyze carefully the structural changes induced by the silylation process, three blanks were prepared by refluxing HAP, HAPD, and NCA solids in toluene overnight, without grafting agent, giving rise to HAP0, HAPD0, and NCA0, respectively, after washing and drying. Chemical analyses of the blanks showed traces of carbon

Table 1 Chemical composition and apparent crystallite sizes of HAP, HAPD, and NCA before and after silane grafting and blank experiments HAP0, HAPD0, and NCA0

Sample	C (wt%)	H (wt%)	N (wt%)	L(002) ( $\pm 3$ Å)	L(310) ( $\pm 3$ Å)
HAP	0.10	0.05	0.09	508	331
HAP0	0.66	0.00	0.00	1054	733
HAP-Si	3.77	0.47	1.23	560	334
HAPD	0.15	0.00	0.00	772	658
HAPD0	0.25	0.21	0.02	1055	746
HAPD-Si	1.81	0.30	0.61	564	319
NCA	0.08	0.52	0.00	238	73
NCA0	1.57	0.58	0.01	294	75
NCA-Si	7.40	1.59	2.30	148	86

Fig. 3 a FTIR spectra of HAP, HAPD, and NCA before grafting. b Decomposition of  $\nu_4$  PO<sub>4</sub> band in FTIR spectra of NCA and HAP

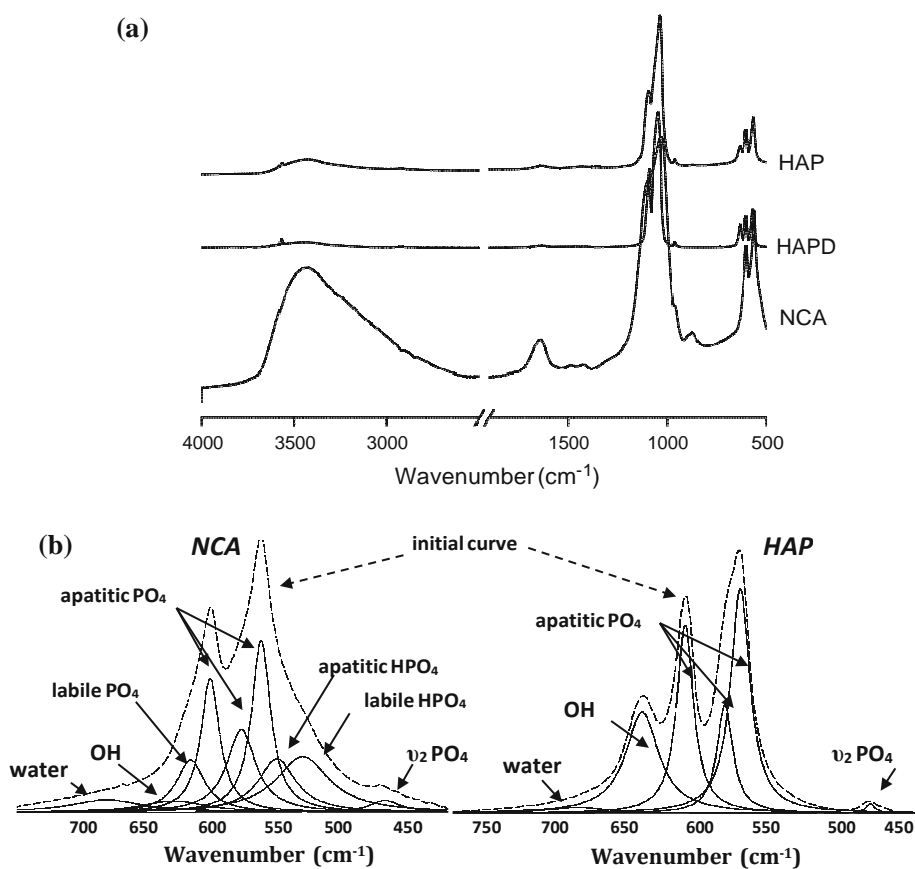
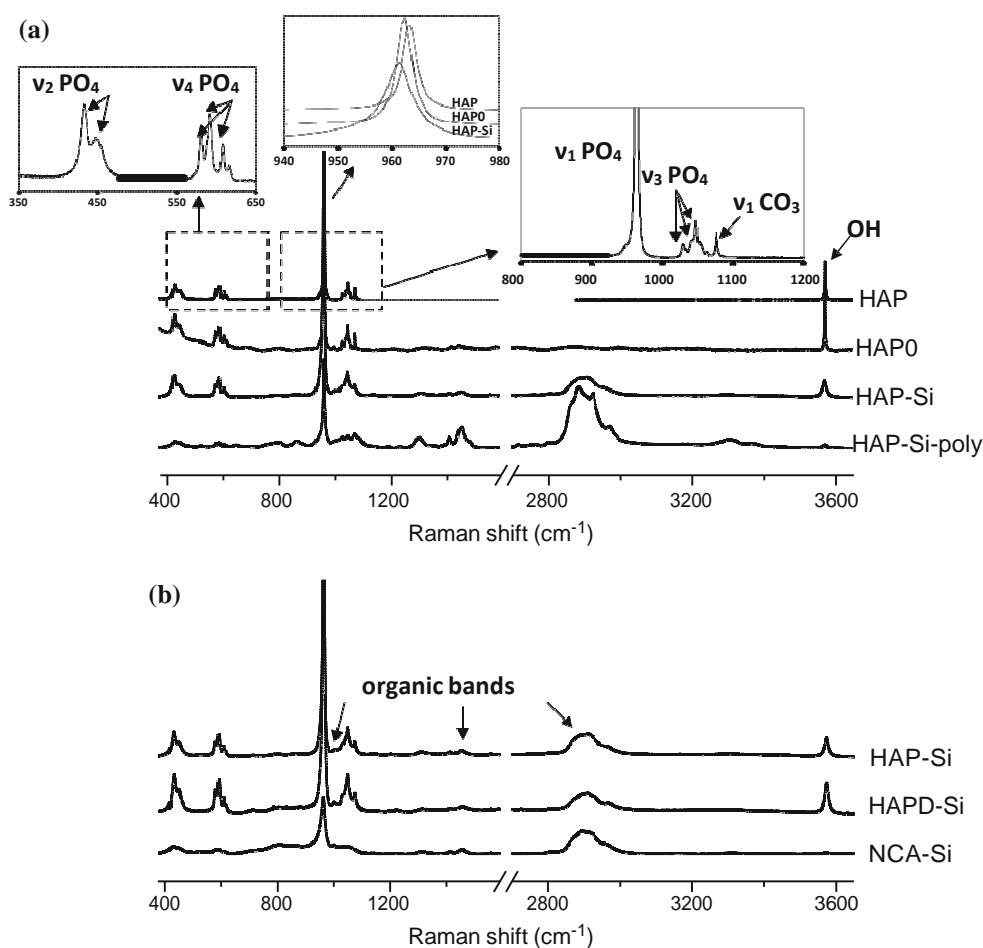


(Table 1) because of toluene adsorption during the reaction. As expected, the carbon, hydrogen, and nitrogen content increased after silylation (grafted APTES), the maximum amount being observed for NCA-Si due to its high specific surface area. One can notice that the initial nitrogen content in the HAP sample disappeared in HAP0 and HAPD. This value can be attributed to ammonia residues from the HAP synthesis. The initial hydrogen content in NCA (about 0.52 wt%) can be attributed to the presence of  $\text{HPO}_4^{2-}$  ions, as observed by FTIR spectrum, which could slightly affect the amount of water calculated

from thermogravimetric analysis. Moreover, carbonate traces in the initial powders confirmed by carbon analysis show that carbonate species still remain after washing and thus could also affect the calculated amount of water.

The XRD diagrams of the blanks (HAP0, HAPD0, and NCA0) displayed better defined diffraction patterns than those of the initial samples (HAP, HAPD, and NCA), as can be seen in Fig. 2b for HAP, in agreement with the increase of the apparent crystallite sizes L(002) and L(310) (Table 1). One can also notice that the crystallite sizes of the samples after silylation decreased compared with the

Fig. 4 Raman spectra of a HAP, HAP0, HAP-Si, and HAP-Si-poly and b HAP-Si, HAPD-Si, and NCA-Si



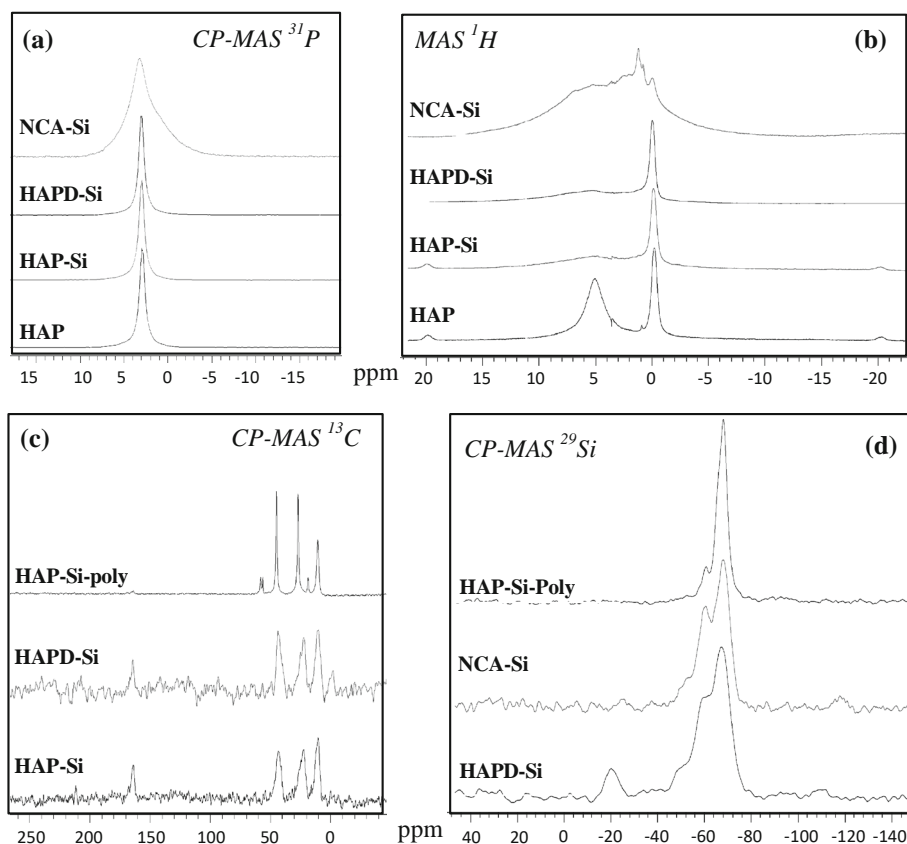
blanks, whatever the initial support. However, the changes observed in the line broadening could also be related to residual stress and the crystallinity of the crystals.

The FTIR spectra of the blanks (HAP0, HAPD0, and NCA0, Fig. 6a) were compared with those of the initial samples (Fig. 3a). For all blanks, a decrease of the  $\text{HPO}_4^{2-}$  vibration band at  $875\text{ cm}^{-1}$  which can be attributed to  $\text{HPO}_4^{2-}$  or  $\text{CO}_3^{2-}$  species (no band observed for the HAPD0 and HAP0 blanks) and a splitting of the  $\text{PO}_4^{3-}$  vibration bands were observed, characteristic of a better apatitic environment in agreement with XRD results. Moreover, for the HAP0 and NCA0 samples, a strong decrease of the intensity of vibration bands attributed to the carbonate species was observed relative to the HAP and NCA samples, probably attributable to the increase of the apatitic environment [18]. At the same time, the decrease of the free water vibration bands could be attributed either to the effect of the temperature or to the influence of toluene, which is known to make an azeotrope with water [33]. For all blank samples, a significant narrowing of the  $\text{OH}^-$  vibration bands at  $630$  and  $3560\text{ cm}^{-1}$  (or appearance in the case of NCA0) was observed and attributed to  $\text{OH}^-$

group formation by drying. Indeed,  $\text{OH}^-$  hydrogen bonding with adsorbed water on apatitic surfaces has been reported to produce signal broadening [34].

After silylation, all FTIR spectra (Fig. 6b) exhibited broader apatitic phosphate bands without shifting and a decrease of the relative intensity of  $\text{OH}^-$  vibration bands of the apatitic structure (disappearance for NCA). For the NCA sample, which exhibited higher silane content, specific APTES bands were observed: new broad bands at  $2950$  and  $2850\text{ cm}^{-1}$  ascribed to asymmetric and symmetric stretching modes of  $\text{CH}_2$  and  $\text{CH}_3$  groups of the aminopropyl chain, respectively [8]; weak bands at  $1460$  and  $1330\text{ cm}^{-1}$  corresponding to asymmetric and symmetric C–H bending deformation bands, respectively [8]; and a series of bands related to N–H stretching modes of the primary amine in the range of  $3500$ – $3000\text{ cm}^{-1}$  and a band owed to the N–H group deformation at  $1620\text{ cm}^{-1}$ , both of which can be overlapped by water vibrations [8, 16, 35]. The characteristic bands of grafted silane were less intense on the HAP-Si and HAPD-Si spectra than on the NCA-Si spectrum because of the lower quantities of grafted silane. The lower silane content in HAP-Si and HAPD-

Fig. 5 CP-MAS  $^{31}\text{P}$  (a) and MAS  $^1\text{H}$  (b) solid NMR spectra of HAP, HAP-Si, HAPD-Si, and NCA-Si. c CP-MAS  $^{13}\text{C}$  solid NMR spectra of HAP-Si, HAPD-Si, and HAP-Si-poly. d CP-MAS  $^{29}\text{Si}$  solid NMR spectra of HAPD-Si, NCA-Si, and HAP-Si-poly



Si was confirmed by microanalysis (Table 1). The expected Si–O–Si, Si–O–C bands (around  $1070\text{ cm}^{-1}$ ), and Si–O–P bands ( $998\text{ cm}^{-1}$ ) could not be observed as they overlapped with strong orthophosphate bands near  $1080\text{ cm}^{-1}$  [16].

Curve fitting in the  $\text{m}_4\text{PO}_4$  domain of the FTIR spectra was carried out for the blanks and the apatitic supports before and after silylation using the GRAMS/386 program (Galactic Industries, Salem, NH). The band shape was considered as Lorentzian and the baseline linear in all instances. Parameters such as the position and width of the bands were varied to provide the best curve fit. The relative band integrated intensities were defined as the ratio between the peak area and the total area of the phosphate bands. Figure 7 reports the relative band integrated intensity for the apatitic OH<sup>-</sup> species. The relative intensity of the OH bands increased in the blanks which presented the highest level of adsorbed water, for HAP0 and especially for NCA0, in agreement with the increase of the apatitic domains observed by XRD. However, the OH<sup>-</sup> band intensity decreased for the two hydroxyapatite samples after silylation, for HAP and especially for the HAPD support which presented the lowest water content and thus the lowest possibility of polycondensation. These results confirm the possibility of silane molecule interaction with OH<sup>-</sup> on apatites.

The Raman spectra of the blanks showed the characteristic vibration bands associated with the orthophosphate, carbonate, and hydroxyl vibrations of the apatitic samples. The relative intensity of the apatitic OH<sup>-</sup> vibration band at  $3570\text{ cm}^{-1}$  appeared stronger in the blanks compared with the initial samples, as observed in Fig. 4A for HAP and HAP0 (data not shown for HAPD and NCA). In all spectra, a shift of the  $\text{m}_1$  ( $960\text{ cm}^{-1}$ ) and  $\text{m}_3$  ( $1040\text{--}1074\text{ cm}^{-1}$ ) modes of  $\text{PO}_4^{3-}$  and of the  $\text{m}_1$  ( $1073\text{ cm}^{-1}$ ) mode of  $\text{CO}_3^{2-}$  was observed for the samples after silylation and for the blanks compared with the initial powders. This can be attributed to the adsorption of toluene, as confirmed by the microanalysis results. However, no hydroxyl band was observed for the NCA0 samples (data not shown). After silylation, the Raman spectra of HAP-Si and HAPD-Si (Fig. 4b) showed a decrease of the OH<sup>-</sup> vibration band intensity at  $3570\text{ cm}^{-1}$ , in accordance with the FTIR results. For all apatitic supports, the carbonate  $\text{m}_1$  vibration band ( $1073\text{ cm}^{-1}$ ) decreased with silane grafting, and the orthophosphate vibration bands appeared broader, which can be attributed to an amorphous structure or to the presence of overlapping organic vibration bands. This is particularly obvious for HAP as shown in Fig. 4a. In Fig. 4b, the spectra of all samples after silylation show an additional broad band at  $2900\text{ cm}^{-1}$  which can be attributed to the CH stretching modes of the  $\text{CH}_2$  and  $\text{CH}_3$

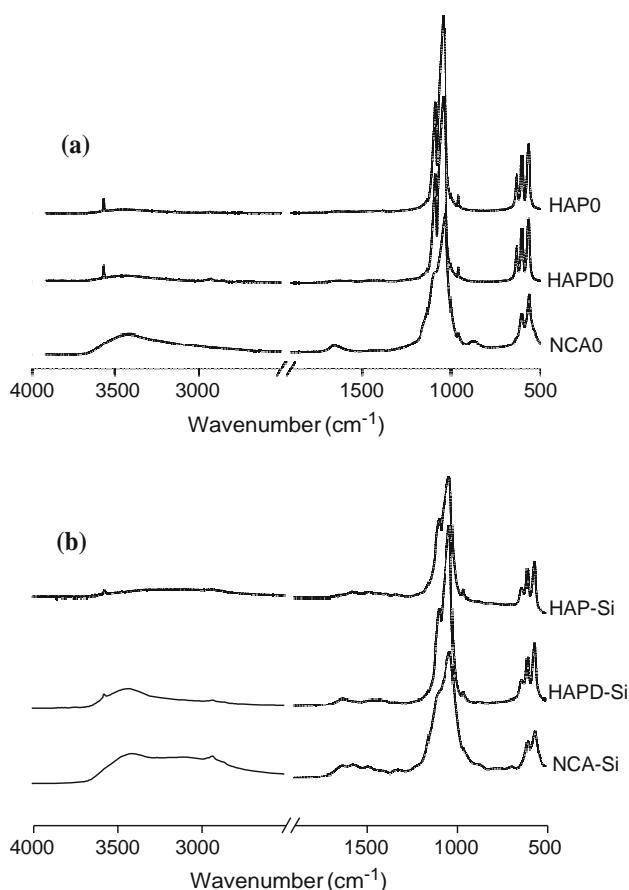


Fig. 6 FTIR spectra of a blank experiments HAP0, HAPD0, and NCA0 and b samples after silylation HAP-Si, HAPD-Si, and NCA-Si

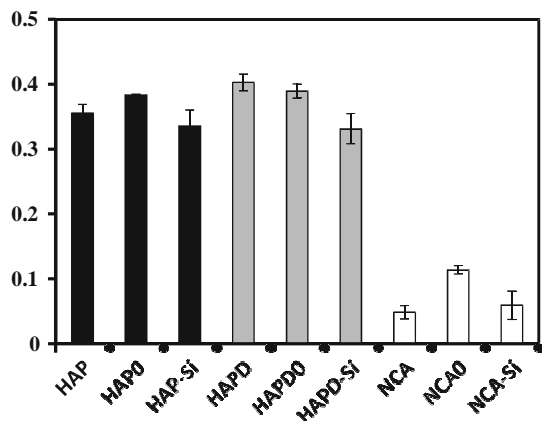


Fig. 7 Relative intensity of FTIR hydroxide bands at  $633\text{ cm}^{-1}$  of apatitic supports before (HAP, HAPD, and NCA) and after silylation (HAP-Si, HAPD-Si, and NCA-Si) and for blank experiments (HAP0, HAPD0, and NCA0)

groups, whereas lower frequency bands between  $1300$  and  $1400\text{ cm}^{-1}$  may correspond to CH vibration modes [36]. Low-intensity broad bands were observed at about  $3300$  and  $1600\text{ cm}^{-1}$  related to the presence of amino groups. Other

small bands between  $600$  and  $650\text{ cm}^{-1}$  were owed to the Si–O–C stretching mode of trialkoxy groups [36, 37], easily observable in the case of the polymerised silane sample HAP-Si-poly obtained by adding water to the toluene. Moreover, a small band appeared at about  $1003\text{ cm}^{-1}$  for the samples after grafting (Fig. 4b). Bands in this region of the spectrum have been attributed in previous studies to the vibrations of the Si–O–P bonds that can form during the reaction of surface phosphate hydroxyl groups with trimethoxysilane groups [17]. However, this band is still present in all blanks' spectra (HAP0 in Fig. 4a, data not shown for HAPD0 and NCA0) and thus cannot be attributed to Si–O–P vibrations. Rather, it appears to be associated with the presence of toluene, probably due to CH vibration bands. Moreover, no hydrolysis was detected by Raman spectroscopy: OH stretching modes of unassociated SiOH groups could not be found in the  $3700$ – $3600\text{ cm}^{-1}$  region, nor Si–O bending vibration of the SiOH group at  $800$ – $650\text{ cm}^{-1}$  [38].

The solid-state MAS  $^1\text{H}$  NMR spectra (Fig. 5b) of the different samples present a signal at  $-0.2\text{ ppm}$  attributed to OH groups. The broader line at  $5.1\text{ ppm}$  (adsorbed water molecules on the surface layer) observed in HAP spectrum before grafting dramatically decreased upon grafting (HAPD-Si, HAP-Si). As the grafting reaction was realised in refluxing dry toluene, which is known to make an azeotrope with water, we suppose that most of the adsorbed water was removed in the initial drying step. For the NCA-Si sample, the NMR spectrum showed numerous broad signals between  $15$  and  $-5\text{ ppm}$  due to a great variety of protons present in the nanocrystals.

The solid-state CP-MAS  $^{31}\text{P}$  NMR spectra of the synthesised apatites before and after silane grafting showed no significant modification (Fig. 5a for HAP). Only one signal was observed at  $3.0\text{ ppm}$  due to orthophosphate species of apatites, as the low number of surface phosphates could not be differentiated from the massive phosphates of the particle core.

The solid-state CP-MAS  $^{13}\text{C}$  NMR spectra of HAP-Si and HAPD-Si samples after silylation are shown in Fig. 5c. Three distinct lines observed at  $10.4$ ,  $22.3$ , and  $43.4\text{ ppm}$  were assigned to carbons C1, C2, and C3: SiCH<sub>2</sub>, CH<sub>2</sub>, and CH<sub>2</sub>NH<sub>2</sub> of the aminopropyl chain, respectively [16, 39]. These signals were more intense in the case of the polymerised silane sample (HAP-Si-poly) obtained by adding water to the toluene, as the carbon content increased, with a slight shift to  $27.0$  and  $44.9$  for C1 and C2 respectively. Moreover, traces of non-hydrolyzed Si–OEt and ethanol were also observed at  $58.1\text{ ppm}$  (–CH<sub>2</sub>OH),  $56.3\text{ ppm}$  (–CH<sub>2</sub>OSi), and  $18.6\text{ ppm}$  (CH<sub>3</sub>) in the polymerised silane sample (HAP-Si-poly). Finally, the signal at around  $164.2\text{ ppm}$  is attributed to carbonate species present in the apatitic samples [18]. These results confirm the presence of APTES on the surface but do not allow conclusions to be drawn on the nature of the silane–solid support interaction.

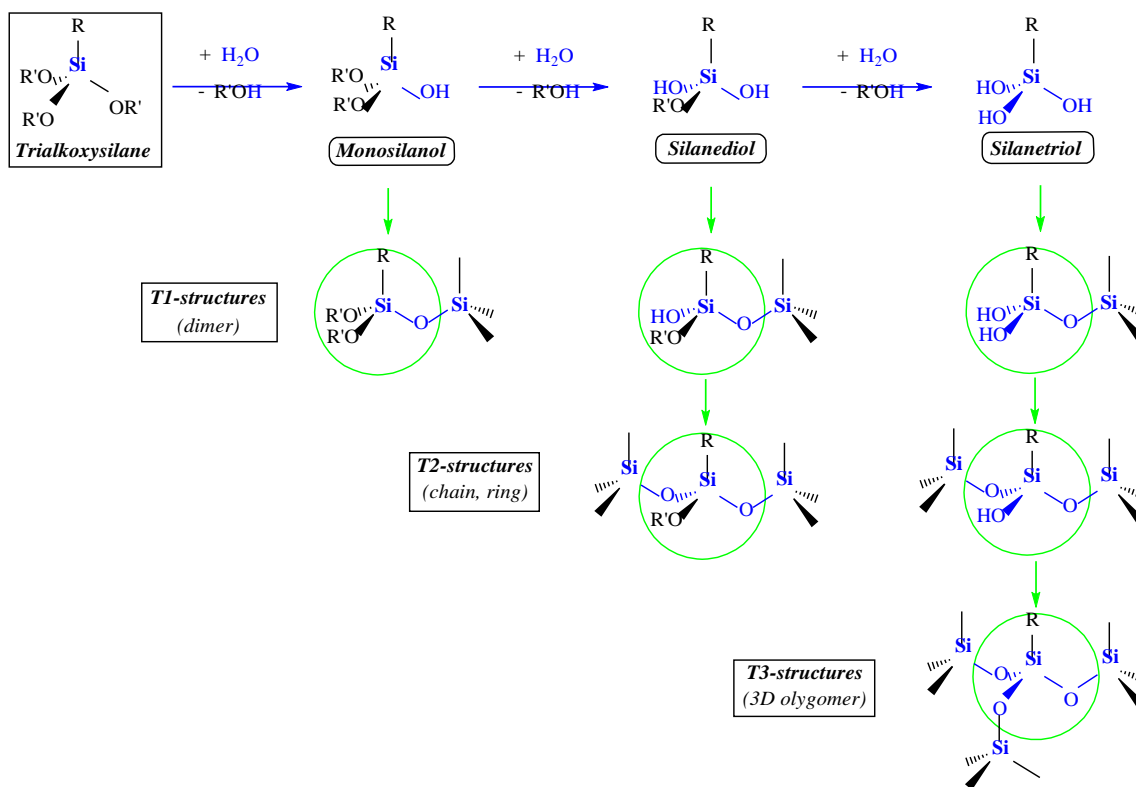
The solid-state CP-MAS  $^{29}\text{Si}$  NMR spectra of the solids after silylation (Fig. 5d HAPD-Si and NCA-Si) showed signals at -50, -60, and -67 ppm attributed, respectively, to the  $T^1$ ,  $T^2$ , and  $T^3$  siloxane structures illustrated in Scheme 1 [16, 40]. In the case of the grafted dried HA (HAPD-Si), the signal at -20.3 was attributed to traces of polysiloxane grease. As expected, the signal of the  $T^3$  structure grew in intensity, relative to those of  $T^1$  and  $T^2$ , on the polymerised sample HAP-Si-poly where this structure is favored. A similar observation can be made for the HAPD-Si and NCA-Si samples but with a lower difference of relative intensity ratio  $T^3/T^2$  compared with the polymerised system. These observations confirm that the  $T^3$  structure is favored by the presence of water as silane hydrolysis allows its polymerisation. This is the reason why alkoxy silane grafting on silica is usually realised under anhydrous conditions to favor alkoxy silane-surface silanol interaction and avoid silane polymerisation.

## Discussion

The data show a clear competition between the covalent grafting of APTES and its polycondensation reaction, in spite of the use of anhydrous organic solvent to avoid surface polymerisation. The TGA data evidenced the presence of water in the apatitic samples, adsorbed water,

or lattice water, more important in the case of the nanocrystalline apatite (NCA sample) than for the hydroxyapatites HAP and HAPD samples (from 4 to 15 wt%) because of the presence of the surface hydrated layer, which participated in the APTES hydrolysis and/or polycondensation. Even after HA pre-drying (HAPD sample), such hydration persisted, not allowing the formation of Si-O-Si related to the polycondensation reaction not to be completely avoided, as the Si-O-Si vibration bands remained present in all spectra. The silane content increased when water content increased in the initial apatitic sample (from HAPD to NCA). No metastable silanol was detected, with its subsequent consumption leading to either grafting or oligomerisation to more stable siloxane (Si-O-Si) probably being immediate.

The blank experiments, performed under the same experimental conditions without surface modification agent, evidence the role of the organic solvent in the silane grafting. The spectroscopic data show a decrease of water content and hydrogen bonding for all blank samples relative to the initial powders. Indeed, toluene is widely used as a carrier for the dehydration of alcohol by azeotropic distillation [33] and thus could extract water from the apatitic samples. This behavior favors the formation of a silane layer by covalent grafting instead of polycondensation. Moreover, a decrease of the line broadening was observed by XRD in the blanks. This phenomenon, never reported in

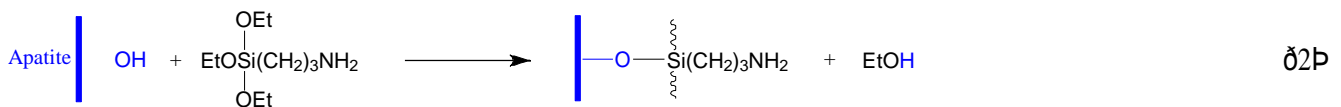


Scheme 1 Different ways of hydrolysis and oligomerisation of trialkoxysilanes

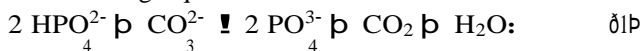
the literature, could be explained by an increase of the crystallite sizes and/or a change on the crystallinity and residual stress in the crystals. These interesting results will be addressed in a further publication.

Although it appears that APTES polycondensation occurs whatever the nature of the apatitic sample, the spectroscopic results evidence at the same time the presence of covalent grafting. APTES covalent grafting is always reported to take place with solid samples through surface OH groups (Solid-OH). Some authors have proposed silane covalent grafting in HAP samples through HPO<sub>4</sub> groups on the basis of spectroscopic results [17]. This hypothesis was supported by the model proposed by Brown for hydroxyapatite structure [41], in which an octacalcium phosphate (OCP, Ca<sub>8</sub>(PO<sub>4</sub>)<sub>4</sub>(HPO<sub>4</sub>)<sub>2</sub>·5H<sub>2</sub>O) layer is present at the surface of the apatitic crystals. The OCP structure can be described as a succession of ‘apatite’ and ‘hydrated’ layers, the latter being rich in HPO<sub>4</sub><sup>2-</sup> ions. OCP could act as a precursor for the formation of HAP with acicular morphology in which the (100) type faces are dominant because they have low interfacial energy. However, in the current study, the IR vibration bands attributed to Si–O–P groups at about 990–1000 cm<sup>-1</sup> [42, 43] cannot be observed, probably because they are overshadowed by

authors have studied silane covalent grafting with hydroxyl groups on the HAP surface without hydrolysis and condensation reaction [44]. In the hexagonal structure of HAP (P6<sub>3</sub>/m space group), the OH<sup>-</sup> ions are present inside tunnels (3 Å of diameter) with the direction parallel to the *c*-axis; each OH<sup>-</sup> ion is coordinated with the three Ca atoms which are arranged in a triangle on the same plane. The OH groups are either above or below the Ca triangle. Depending on the surface crystallographic planes, the binding energies and the planar atomic density differ and have been calculated by Zhang et al. [44] using molecular dynamic simulations: the (100) and (110) planes exhibit the highest planar OH<sup>-</sup> density (atom 0.072 Å<sup>-2</sup>), and the (110) plane displays the highest planar energy for methacryloxypropyl trimethoxy silane. In addition, for NCAs, Blumenthal and Posner [34] have suggested that some OH<sup>-</sup> ions present in the solids cannot be observed by FTIR spectroscopy because of hydrogen bonding with water molecules in the hydrated surface layer. Thus, the results obtained lead to the conclusion that silylation can be explained at the same time by APTES polycondensation and covalent grafting to oxygen atom of the hydroxyl groups of the apatitic structure and/or the OH<sup>-</sup> species that are present on the surface hydrated layer according to Eq. 2:



Si–O–Si, Si–O–C (1070 cm<sup>-1</sup>), and PO<sub>4</sub><sup>3-</sup> vibration bands at 1000–1100 cm<sup>-1</sup> (no shift of the PO<sub>4</sub><sup>3-</sup> vibration bands was observed). Moreover, some authors have associated the appearance of a Raman vibration band at 900–1000 cm<sup>-1</sup> after silylation with Si–O–P vibrations [17], but these bands were already observed in the spectra of the blank samples and thus can be attributed to vibrations of organic solvent. In addition, the decrease of the HPO<sub>4</sub><sup>2-</sup> FTIR vibration band at 875 cm<sup>-1</sup> observed after APTES grafting was also observed in the spectra of the blanks, correlated with the decrease of CO<sub>3</sub><sup>2-</sup> species according to the following Eq. 1:



Thus, APTES covalent grafting through the hydroxyl groups of surface HPO<sub>4</sub> groups cannot be confirmed.

On the other hand, a clear positive marker in favor of silylation is the decrease of OH<sup>-</sup> apatitic species. The decrease of hydroxyl species appears higher in HAPD after drying than HAP, presenting the lowest amount of water and thus the weakest possibility of polycondensation. Some

It can be noticed that an ion-exchange process cannot be proposed to explain APTES grafting on the apatitic solids as the experiments were performed in toluene without aqueous medium. In order to favor APTES covalent grafting, the use of anhydrous solvents and pre-drying of the apatitic samples are necessary. However, even under these conditions it is impossible to avoid silane polymerisation completely on solid surfaces. With the aim of their use in heterogeneous catalysis, further experiments have to be performed on the solids after grafting to study the efficiency of such system and the stability of the layer obtained in catalytical conditions.

## Conclusion

APTES grafting was performed in toluene on different apatitic supports. Different supports were prepared: crystallised stoichiometric hydroxyapatites differing by the drying method, freeze-dried (HAP) and dried at 100 °C (HAPD), and an NCA. All materials were fully

characterised, before and after grafting, for better understanding of the nature of the alkoxy silane/surface interaction.

The data show a clear competition between the covalent grafting of APTES and its polycondensation reaction, depending on the nature of the solid support surface, in spite of the use of anhydrous organic solvent to avoid surface polymerisation. Generally, polycondensation is favored by a more hydrated surface, whereas covalent bonding necessitates dry conditions. In this paper, although it appears that APTES polycondensation occurs whatever the nature of the apatitic sample, the spectroscopic results evidence at the same time the presence of covalent grafting. Alkoxy silane covalent grafting is always reported to take place with solid samples through surface OH groups (Solid-OH). In the current study, the IR vibration bands attributed to Si–O–P groups could not be observed, so APTES covalent grafting through the hydroxyl groups of surface HPO<sub>4</sub> groups cannot be confirmed. However, a clear and positive marker in favor of covalent grafting is the decrease of OH<sup>-</sup> apatitic species, highest on the apatitic support presenting the lowest amount of water (HAPD) and thus the weakest possibility of polycondensation. The results obtained lead to the conclusion that silylation can be explained at the same time by APTES polycondensation and by APTES covalent grafting to oxygen atom of the hydroxyl groups of the apatitic structure and/or of the OH<sup>-</sup> species that are present on the surface hydrated layer.

This work clarifies the nature of silane grafting onto selected apatitic surfaces and especially the influence of the composition and properties of the apatitic surfaces on the process of silylation. In order to favor covalent grafting of alkoxy silanes, the use of anhydrous solvents and pre-drying of the apatitic samples are necessary. However, even under these conditions it is impossible to avoid silane polymerisation completely on the solid surfaces. The understanding of the nature of silane–surface interactions provides fundamental tools for the development of novel solid supports for heterogenous catalytic applications.

## References

1. Fechete I, Wang Y, Védrine JC (2012) The past, present and future of heterogeneous catalysis. *Catal Today* 189(1):2–27
2. Drouet C, Bosc F, Banu M, Largeot C, Combes C, Dechambre G et al (2009) Nanocrystalline apatites: from powders to biomaterials. *Powder Technol* 190(1–2):118–122
3. Sarda S, Fernandez E, Nilsson M, Balcells M, Planell JA (2002) Kinetic study of citric acid influence on calcium phosphate bone cements as water-reducing agent. *J Biomed Mater Res* 61(4):653–659
4. Grossin D, Rollin-Martinet S, Estournès C, Rossignol F, Champion E, Combes C et al (2010) Biomimetic apatite sintered at very low temperature by spark plasma sintering: physico-chemistry and microstructure aspects. *Acta Biomater* 6(2):577–585
5. Yin G, Liu Z, Zhan J, Ding F, Yuan N (2002) Impacts of the surface charge property on protein adsorption on hydroxyapatite. *Chem Eng J* 87(2):181–186
6. Autefage H, Briand-Mésange F, Cazalbou S, Drouet C, Fourmy D, Gonçalves S et al (2009) Adsorption and release of BMP-2 on nanocrystalline apatite-coated and uncoated hydroxyapatite/b-tricalcium phosphate porous ceramics. *J Biomed Mater Res B Appl Biomater* 91B(2):706–715
7. Al-Kattan A, Errassifi F, Sautereau AM, Sarda S, Dufour P, Barroug A et al (2010) Medical potentialities of biomimetic apatites through adsorption, ionic substitution, and mineral/organic associations: three illustrative examples. *Adv Eng Mater* 12(7):B224–B233
8. Da Silva OG, Da Silva Filho EC, Da Fonseca MG, Arakaki LNH, Airoldi C (2006) Hydroxyapatite organofunctionalized with silylating agents to heavy cation removal. *J Colloid Interface Sci* 302(2):485–491
9. Kawasaki T (1991) Hydroxyapatite as a liquid chromatographic packing. *J Chromatogr A* 544:147–184
10. Tahir R, Banert K, Solhy A, Sebti S (2006) Zinc bromide supported on hydroxyapatite as a new and efficient solid catalyst for Michael addition of indoles to electron-deficient olefins. *J Mol Catal A: Chem* 246(1–2):39–42
11. Smahi A, Solhy A, El Badaoui H, Amoukal A, Tikad A, Maizi M et al (2003) Potassium fluoride doped fluorapatite and hydroxyapatite as new catalysts in organic synthesis. *Appl Catal A* 250(1):151–159
12. Damia C, Sarda S, Deydier E, Sharrock P (2004) Study of two hydroxyapatite/poly(alkoxy silane) implant coatings. *Surf Coat Technol* 201(6):3008–3015
13. Durrieu MC, Pallu S, Guillemot F, Bareille R, Amédée J, Baquey C et al (2004) Grafting RGD containing peptides onto hydroxyapatite to promote osteoblastic cells adhesion. *J Mater Sci* 15(7):779–786. doi:10.1023/B:JMSM.0000032818.09569.d9
14. Kim J, Seidler P, Wan LS, Fill C (2009) Formation, structure, and reactivity of amino-terminated organic films on silicon substrates. *J Colloid Interface Sci* 329(1):114–119
15. Simon A, Cohen-Bouhacina T, Porté MC, Aimé JP, Baquey C (2002) Study of two grafting methods for obtaining a 3-aminopropyltriethoxysilane monolayer on silica surface. *J Colloid Interface Sci* 251(2):278–283
16. Goonasekera CS, Jack KS, Cooper-White JJ, Grondahl L (2013) Attachment of poly(acrylic acid) to 3-aminopropyltriethoxysilane surface-modified hydroxyapatite. *J Mater Chem B* 1(42):5842–5852
17. Vasiliev AN, Zlotnikov E, Khinast JG, Riman RE (2008) Chemisorption of silane compounds on hydroxyapatites of various morphologies. *Ser Mater* 58(12):1039–1042
18. Eichert D, Drouet C, Sfihi H, Rey C, Combes C (2007) Nanocrystalline apatite-based biomaterials: synthesis, processing and characterization. In: Kendall JB (ed) *Biomaterials research advances*. Nova Science Publishers, New York, pp 93–143
19. Liu Q, De Wijn JR, De Groot K, Van Blitterswijk CA (1998) Surface modification of nano-apatite by grafting organic polymer. *Biomaterials* 19(11–12):1067–1072
20. Toworfe GK, Composto RJ, Shapiro IM, Ducheyne P (2006) Nucleation and growth of calcium phosphate on amine-, carboxyl- and hydroxyl-silane self-assembled monolayers. *Biomaterials* 27(4):631–642
21. Trombe JC (1972) Contribution à l'étude de la décomposition et la réactivité de certaines apatites hydroxylées carbonatées ou fluorées alcalino-terreuses. PhD Thesis, UPS, Toulouse, France
22. Rey C, Hina A, Tofighi A, Glimcher MJ (1995) Maturation of poorly crystalline apatites: chemical and structural aspects in vivo and in vitro. *Cells Mater* 5(4):345–356

23. Sakeye M, Smått J-H (2012) Comparison of different amino-functionalization procedures on a selection of metal oxide microparticles: degree of modification and hydrolytic stability. *Langmuir* 28(49):16941–16950
24. Charlot G (1974) *Chimie analytique quantitative*. Masson et Cie, Paris
25. Guinier A (1960) *Théorie et technique de la radiocristallographie*, 3rd edn. Dunod, Paris
26. Ashok M, Meenakshi Sundaram N, Narayana Kalkura S (2003) Crystallization of hydroxyapatite at physiological temperature. *Mater Lett* 57(13–14):2066–2070
27. Heughebaert JC (1977) Contribution à l'étude de l'évolution des orthophosphates de calcium précipités amorphes en orthophosphates apatitiques. PhD Thesis, INP Toulouse
28. Elliott JC (1994) Structure and chemistry of the apatites and other calcium orthophosphates. Elsevier, Amsterdam
29. Rey C, Combes C, Drouet C, Lebugle A, Sfihi H, Barroug A (2007) Nanocrystalline apatites in biological systems: characterisation, structure and properties. *Materialwiss Werkstofftech* 38(12):996–1002
30. Penel G, Leroy G, Rey C, Bres E (1998) MicroRaman spectral study of the PO<sub>4</sub> and CO<sub>3</sub> vibrational modes in synthetic and biological apatites. *Calcif Tissue Int* 63(6):475–481
31. Yesinovski JP, Eckert H (1987) Hydrogen environments in calcium phosphates: <sup>1</sup>H MAS NMR at high spinning speeds. *J Am Chem Soc* 109:6274–6282
32. Jäger C, Welzel T, Meyer Zaika W, Epple M (2006) A solid state NMR investigation of the structure of nanocrystalline hydroxyapatite. *Magn Reson Chem* 44(6):573–580
33. Gomis V, Font A, Saquete MD (2008) Homogeneity of the water ? ethanol ? toluene azeotrope at 101.3 kPa. *Fluid Phase Equilib* 266(1–2):8–13
34. Blumenthal N, Posner A (1973) Hydroxyapatite: mechanism of formation and properties. *Calcif Tissue Res* 13(1):235–243
35. Domingo C, Loste E, Fraile J (2006) Grafting of trialkoxysilane on the surface of nanoparticles by conventional wet alcoholic and supercritical carbon dioxide deposition methods. *J Supercrit Fluids* 37(1):72–86
36. Bistričić L, Volovšek V, Dananić V (2007) Conformational and vibrational analysis of gamma-aminopropyltriethoxysilane. *J Mol Struct* 834–836:355–363
37. Ishida H, Chiang C, Koenig JL (1982) The structure of amino-functional silane coupling agents: 1. c-Aminopropyltriethoxysilane and its analogues. *Polymer* 23(2):251–257
38. Shih PTK, Koenig JL (1975) Raman studies of the hydrolysis of silane coupling agents. *Mater Sci Eng* 20:137–143
39. Sharma RK, Pandey A, Gulati S (2012) Silica-supported molybdenum complex: a novel, selective and reusable organic–inorganic hybrid catalyst for eco-friendly oxidation of sulfides and olefins. *Polyhedron* 45(1):86–93
40. Cardiano P, Sergi S, Lazzari M, Piraino P (2002) Epoxy–silica polymers as restoration materials. *Polymer* 43(25):6635–6640
41. Brown WE, Mathew M, Chow LC (1984) Roles of octacalcium phosphate in surface chemistry of apatites. In: Misra D (ed) *Adsorption on and surface chemistry of hydroxyapatite*. Springer, New York, pp 13–28
42. Wang X, Song G, Lou T (2010) Fabrication and characterization of nano-composite scaffold of PLLA/silane modified hydroxyapatite. *Med Eng Phys* 32(4):391–397
43. Zhang SM, Liu J, Zhou W, Cheng L, Guo XD (2005) Interfacial fabrication and property of hydroxyapatite/poly lactide resorbable bone fixation composites. *Curr Appl Phys* 5(5):516–518
44. Zhang H-p LuX, Leng Y, Fang L, Qu S, Feng B et al (2009) Molecular dynamics simulations on the interaction between polymers and hydroxyapatite with and without coupling agents. *Acta Biomater* 5(4):1169–1181